Research on Engineering Structures & Materials
www.jresm.org

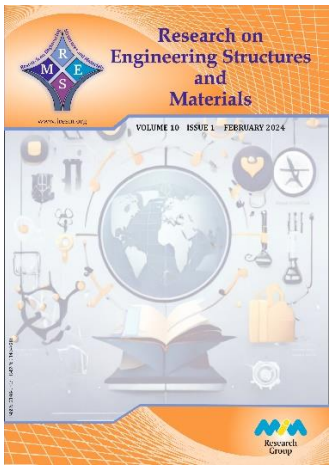


# Prediction of forming limit diagrams for steel sheets with an artificial neural network and comparison with empirical and theoretical models

Cengiz Görkem Dengiz, Fevzi Şahin

Online Publication Date: 30 November 2023
URL: http://www.jresm.org/archive/resm2023.32ma0825rs.html
DOI: http://dx.doi.org/10.17515/resm2023.32ma0825rs

Journal Abbreviation: *Res. Eng. Struct. Mater.*

**To cite this article**
Dengiz CG, Sahin F Prediction of forming limit diagrams for steel sheets with an artificial neural network and comparison with empirical and theoretical models. *Res. Eng. Struct. Mater.*, 2024; 10(2): 651-677.

Research on Engineering Structures & Materials
www.jresm.org
Research Group

*Research Article*

# Prediction of forming limit diagrams for steel sheets with an artificial neural network and comparison with empirical and theoretical models

Cengiz Görkem Dengiz*,[a], Fevzi Şahin[b]

*Department of Mechanical Engineering, Ondokuz Mayıs University, Samsun, Türkiye*

**Article Info**

*Article history:*

Received 25 Aug 2023
Accepted 21 Nov 2023

*Keywords:*

*Formability;*
*Artificial neural network;*
*Forming limit diagram;*
*Steel sheets;*
*Sheet metal forming*

**Abstract**

The automotive industry heavily relies on forming limit diagrams (FLDs) as essential tools for ensuring the quality and manufacturability of sheet metal components. However, accurately determining FLDs can be complex and resource-intensive due to the numerous material properties and variables involved. To address this challenge, this research employs an artificial neural network (ANN) model to predict FLDs for sheet metals, explicitly focusing on the automotive sector. The study begins by gathering material properties, including sheet thickness, yield strength, ultimate tensile strength, uniform elongation, hardening exponent, and strength coefficient. These properties serve as crucial inputs for the ANN model. Sensitivity analysis is then conducted to discern how each parameter influences FLD predictions. The ANN model is meticulously constructed, with a 6-15-22-3 structure, and subsequently trained to predict FLDs. The results are promising, as the model achieves an exceptional R-value of 0.99995, indicating high accuracy in its predictions. Comparative analysis is carried out by pitting the ANN-generated FLDs against experimental data. The findings reveal that the ANN model predicts FLDs with remarkable precision, exhibiting only a 3.4% difference for the FLD0 value. This level of accuracy is particularly significant in the context of automotive manufacturing, where even minor deviations can lead to substantial product defects or manufacturing inefficiencies. It offers a swift and reliable way of predicting FLDs, which can be instrumental in optimising manufacturing processes, reducing material waste, and ensuring product quality. In conclusion, this research contributes to the automotive manufacturing sector by providing a robust and efficient method for predicting FLDs.



## 1. Introduction

The limits of that material should be determined to use the material in forming operations with maximum efficiency. These material limits are known as formability. Sheet metal formability is defined as the ability of the metal to deform into a desired shape without necking or fracture [1]. These limits for sheet metals in forming operations are expressed by the forming limit diagram (FLD). Keeler and Goodwin first introduced this concept in the 1960s [2,3]. Keeler studied the right side of the diagram while Goodwin examined the left side (Fig. 1). In Fig. 1, the vertical axis shows the major strain ($\varepsilon_1$), and the horizontal axis shows the minor strain ($\varepsilon_2$) on sheet metal. The forming limit as a function of the strain state can be presented as a curve in a $\varepsilon_1$-$\varepsilon_2$ diagram. That kind of diagram is called the forming limit diagram (FLD), and the curve is called the forming limit curve (FLC) [4]. The $FLC_0$ value is the major strain value at which the minor strain value is 0 in the FLC. This value is also known as the lowest point of the FLC. According to this diagram, the area

*Corresponding author: gorkem.dengiz@omu.edu.tr
[a] orcid.org/0000-0003-1308-3223; [b] orcid.org/0000-0002-4808-4915
DOI: http://dx.doi.org/10.17515/resm2023.32ma0825rs

under the FLC shows the safe margin; the area above the curve shows where fracture will occur. In other words, as long as the major and minor deformations in the sheet metal fall below this curve, no necking or fracture will occur. If the deformations are higher than the limit strains of the FLC, the sheet metal will be necked or fractured.

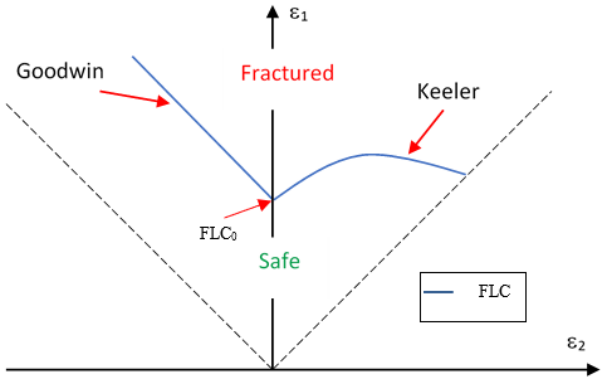


Fig. 1. Schematic forming limit diagram (FLD) found by Keeler and Goodwin [5]

The deformations during the sheet metal forming process are determined using the finite element method and compared with the FLC. Successful products are obtained by changing the material or design in areas with high or critical deformation. There are many experimental and theoretical studies and models for determining FLCs. The FLC can be determined by various methods such as the uniaxial tensile test [6], the hydraulic dome test [7], the Keeler test [2], the Hecker test [8], the Marciniak test [9], the Nakajima test [10] and the Hasek test [11]. In these experimental methods, FLCs can be determined using different specimens and tools [12]. The most commonly used tests are the Nakajima and Marciniak tests. In these tests, the FLC's left and right parts are obtained using specimens of different widths and types. However, experimental methods are costly due to the need for special devices and tools, and the preparation and measurement of test specimens are also time-consuming. Therefore, many theoretical and numerical models have been developed for the calculation of the formability of sheet metals.

Theoretical and numerical models are based on geometric imperfection theory, continuum mechanics and bifurcation theory. The most well-known of these models are the Marciniak–Kuczynski criterion [13], the Swift and Hill model [14,15] and the Gurson–Tvergaard–Needleman [16] model. In these models, quadratic or linear equations are solved with the parameters of the materials and the FLC is obtained. All these models and other empirical methods are summarised by Zhang et al. [17].

Although there are many studies in the literature in which experimental methods and theoretical models determine FLC, statistical analyses on this subject are limited. However, these experimental and theoretical studies guide the researchers by giving information about the factors affecting the FLC. Subramani et al. [18] experimentally determined FLCs for three different thicknesses of three other aluminium alloys and modelled them with the Taguchi experimental design. They determined the mechanical properties, such as yield strength and hardening exponent, using tensile tests. They used this data as a variable in the Taguchi experimental design and used the forming limit strain values as outputs. As a result of the study, they showed that the data obtained from the tensile tests can be used in the estimation of the FLC. They also found that the most critical factors affecting the FLC are the strain hardening exponent and normal anisotropy. Paul [19] created a statistical model that predicts $FLC_0$ point by processing data such as the tensile strength, elongation, strain hardening and thickness of steel materials collected from the literature. To estimate

this point, the author created a model by processing the data from 66 types of steel in total. With this model, forming limit stress diagrams (FLSDs) was predicted with a high success rate. Levy and Van Tyne [20] also developed a method for predicting FLSDs. They calculated the effective stress in the $FLC_0$ value with a Z parameter created with tensile test data from the literature. They also computed FLSDs for the left side of the FLC. A more comprehensive investigation of the controlling factors of FLC can be found in [21].

Forming Limit Diagrams (FLDs) are of paramount significance in the automotive industry, acting as a linchpin in the manufacturing process of sheet metal components. These diagrams are critical guides ensuring automotive parts' quality and structural integrity. However, their accurate determination is a formidable challenge. With stringent quality standards and cost-efficiency imperatives, the automotive industry relies heavily on precise FLDs. Minor deviations in these diagrams can lead to defects in the final product, escalating production costs and causing delays. Traditional methods of FLD determination are often limited by empirical or theoretical models, which may not encompass the intricate variations introduced during the production process. As a result, there is an escalating need for predictive models that can bridge this gap and offer an accurate means of determining FLDs. In recent times, artificial neural networks (ANNs) have been used frequently in metal forming processes. These advanced models can potentially revolutionise how FLDs are predicted, offering an innovative solution to the challenges faced by the automotive industry and other sectors that rely on sheet metal forming. Many researchers have used system theoretical models to model the system and reduce their experimental work. The ANN method, which has recently become popular, is a modelling method that can be applied to almost any engineering system. Since ANNs have many different models and learning algorithms, they can be applied to other systems. An ANN is a modelling method that tries to learn and use the relationship between input and output variables without considering the underlying physical processes. The relationship between inputs and outputs can be formulated. The effects of the inputs can be seen through the outputs using an ANN. With all these superior aspects, ANNs have been the basis for many studies in sheet-metal forming processes. Kotkunde et al. [22] modelled the deep drawing process of Ti-6Al-4V alloy using an ANN method. They used parameters such as blank holder force (BHF), punch speed and temperature as inputs. They could predict the major and minor strains with an ANN by processing the simulation results as outputs. They also plotted the FLC with the Keeler formula using the major and minor strain values obtained from the simulation. Elangovan et al. [23] modelled the FLC of perforated pure aluminium sheets with an ANN. They experimentally determined major and minor strain values by forming perforated sheets of different widths. Using sheet widths and hole sizes as inputs, they trained the network and obtained major and minor strain values that agreed with the experimental data. Derogar and Djavanroodi [24] experimentally determined the FLCs of Ti6Al4V titanium alloy and Al6061-T6 aluminium alloy sheets using the Hecker test. They gave punch displacement, oil pressure and limit drawing ratios (LDR) to the ANN as inputs and obtained FLC values as outputs. They got a high similarity between the experimental and ANN data. They found that FLCs can be successfully predicted by an ANN. Forcellese et al. [25] tried to predict the yield curves and FLCs of AZ31 magnesium alloys with experimental measurements and an ANN. They used parameters such as temperature, minor strain, forming speed and rolling direction as inputs for predicting the FLCs. They showed that the ANN can predict FLCs accurately, although no information was provided about the complex mechanisms involved in microstructure during hot forming. Dehghani et al. [26] investigated the effect of thermomechanical properties of low-carbon steels on the FLC with an ANN. In their model, the carbon content, hot finishing temperature, strain hardening exponent, initial yield stress and ASTM grain size were inputs and used to predict the FLC as an output. They reported that the FLC indicated with these thermomechanical properties was highly compatible with the experimentally

obtained FLC. All of these studies found that the FLC can be predicted with an ANN successfully for a specific material in which experimental parameters or material properties are given as input. Although FLC can be successfully estimated for the sheet used in the study, creating a new ANN for different steel sheets is necessary. Therefore, there is a need for an ANN in which the FLCs of other steel sheets can be determined by simply giving their material properties.

This article delves into the development and application of ANNs for predicting FLDs in the automotive sector. It explores the implications of accurate predictions on manufacturing processes, product quality, cost efficiency, and, most importantly, safety. As the industry navigates the ever-evolving landscape of materials and design, predictive models like ANNs offer a bridge between innovation and reliability, contributing to producing safer, more efficient, and environmentally responsible vehicles. In this study, an ANN model has been developed to predict the whole FLCs of different steel sheets. Mechanical properties found in any material database are given as input. In this context, the yield stress, tensile strength, strain hardening exponent, strength coefficient, uniform elongation and thickness values of steel materials collected from different studies and experimental studies are inputs to the ANN. The FLCs of the steel sheets were processed as the output with data from the uniaxial, plane strain and biaxial regions. This ANN model can obtain the FLC of the different steel sheets for which the mechanical properties are given as inputs.

## 2. Materials and Methods

### 2.1. Materials

In this study, DC01 was used for experiments. The thickness of the sheet metals is 0.6 mm. The chemical contents of the selected material are given in Table 1. These chemical contents are based on the material standards. The tensile test was used to determine the mechanical properties of the material, and out-of-plane tests were used to determine the FLC.

Table 1. Chemical composition of DC01 sheet metal [27]

| Material | %C | %P | %S | %Mn | %Fe |
|---|---|---|---|---|---|
| DC01 | 0.12 | 0.045 | 0.045 | 0.6 | 99.19 |

### 2.2 Tensile Test

Tensile test specimens were prepared following the ASTM E8 [28] standard to determine the mechanical properties of the steel sheet. Specimens that cut parallel, diagonal and perpendicular with respect to the rolling direction were tested using an Instron 5982, which has 100 kN loading capacity. All tests were performed at a constant head speed of 10 mm/min until fracture occurred and were repeated a minimum of 3 times to minimise deviations in results. A standard mechanical extensometer with a length of 50 mm was used to measure the strain accurately. The material's strain hardening exponent and strength coefficient were determined by linear regression analysis on the true stress–true strain curves on a logarithmic scale. The yield stress, tensile stress, elongation and strain hardening exponent obtained as a result of tensile tests are given in Table 2.

Table 2. Mechanical properties of DC01 sheet metal

| Mechanical Properties | DC01 |
|---|---|
| Elastic modulus, $E$ (GPa) | 194.7 |
| Yield stress, $R_{p0,2}$ (MPa) | 204.3 |
| Tensile stress, $R_m$ (MPa) | 335.9 |
| Uniform elongation, $\varepsilon$ (mm/mm) | 0.241 |
| Max. elongation, $\varepsilon_{max}$ (mm/mm) | 0.406 |
| Strain hardening coefficient, $n$ | 0.212 |
| Strength coefficient, $K$ (MPa) | 576.3 |

### 2.3 Out-of-plane Tests

To determine the FLC of the material, it should be formed under different strain conditions. Therefore, specimens of various widths that are usually compressed between a die and a blank holder are stretched with a hemispherical punch until they are necked or fractured (Fig. 2a). The dimensions of the die are given in Fig. 2b. A double-acting hydraulic press with a loading capacity of 80 tonnes was used for the out-of-plane test. After closing the die and blank holder, a 90 kN clamping force was applied. Nylon film and mineral oil are used between the sheet metal and punch to prevent premature damage from friction.

In this study, sheet metals of eight different widths, as shown in Fig. 3a, were formed by a hemispherical punch until they fractured. The specimen dimensions are given in detail by Ozturk and Lee [1]. Circular grids with a diameter of 2.5 mm were electrochemically etched onto the sheets before forming (Fig. 3a). Each sample represents one strain path from uniaxial to biaxial strain on the FLD. After the experiments, these grids changed shape from circular to elliptical, and optical grid measurements were used to determine the major and minor strains. The FLCs were obtained by plotting these values on a graph [29]. Fig. 3b shows the fractured specimens after the experiment.

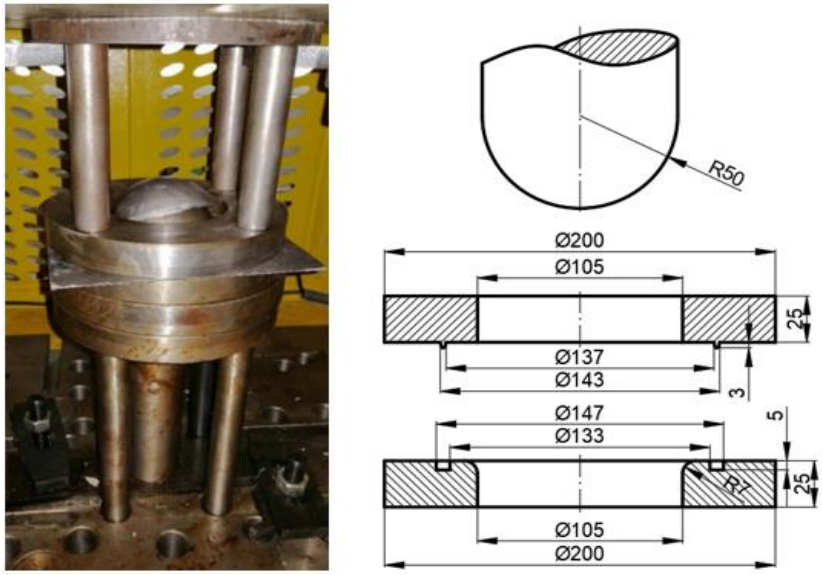


(a) (b)

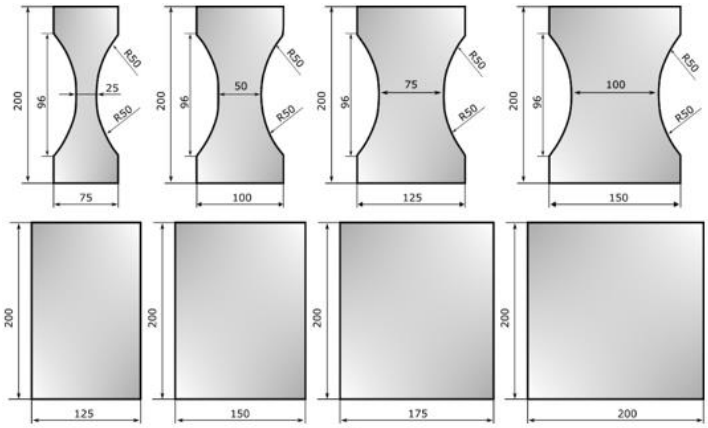


(c)

Fig. 2. (a) Fractured sample in out-of-plane test (b) Technical drawing of the out-of-plane test setup (c) Specimen dimensions (all dimensions are mm)

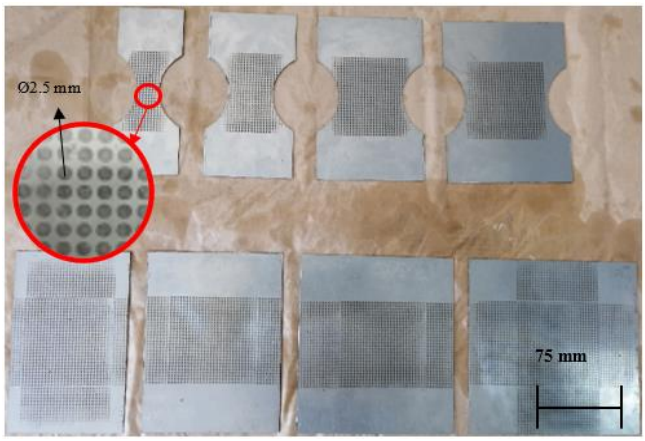


(a)

(b)

Fig. 3. Out-of-plane test specimens (a) before and (b) after the test

After the samples were deformed, the deformations on the sheet surfaces were measured with camera-integrated image processing software (Fig. 4a). Each deformed ellipse where the damage occurred on the sheet surface was photographed with the camera. Later, these photographs were transferred to the image processing program, and the major and minor axes of the ellipses were measured (Fig. 4b). In the program, the circles etched on the sheet metal were displayed with the camera before deformation. The program is calibrated by measuring the diameter of the reference circle over these images. After deformation, the ellipses, whose axis lengths are measured, are proportional to the reference circle size and the true strains are calculated. Here, measuring the ellipses from the same distance each time while viewing is essential for the consistency of the measurements.

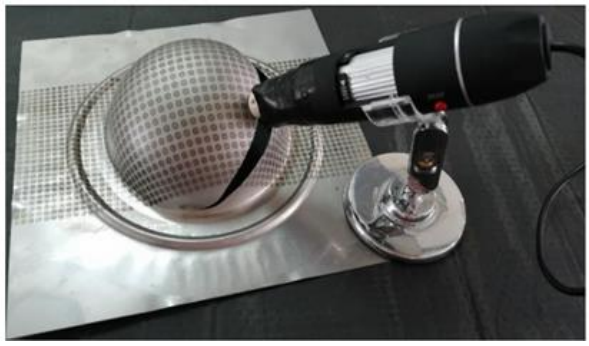

(a)

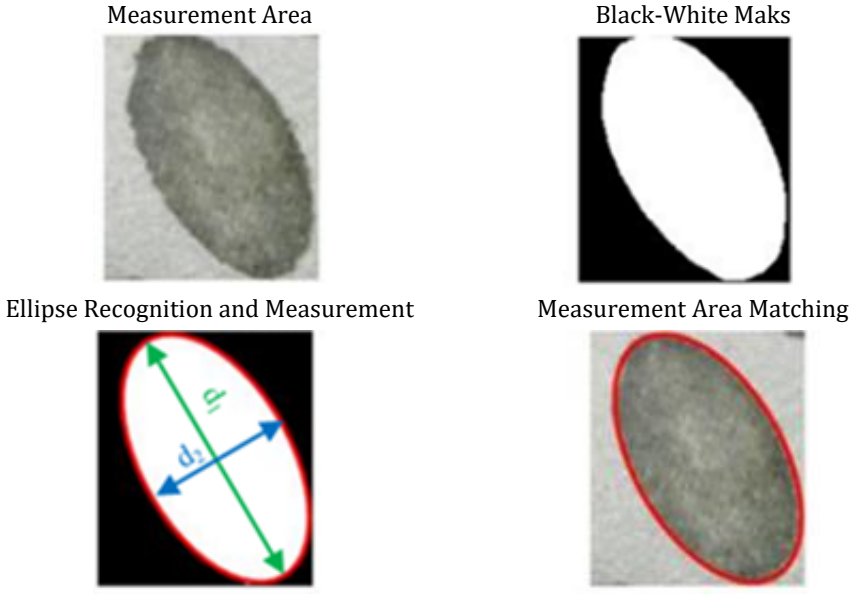


(b)

Fig 4. Determination of major and minor strain (a) Taking a picture with a camera (b) Measurement with image processing

The damaged area of each deformed sample was examined, and the ellipses to be measured were determined and photographed. As a result of the measurements, the major ($\varepsilon_1$) and minor ($\varepsilon_2$) true strains were calculated with the equations (1) and (2). The major true strain was calculated by measuring the long axes of the ellipses on the sheet, and minor true strains were calculated by measuring their short axes. In equations (1) and (2), the

diameter of the circle before deformation is $d_0$, the major axis of the ellipse formed after deformation is $d_1$, and the minor axis is $d_2$.

$$\varepsilon_1 = ln\frac{d_1}{d_0} \quad (1)$$

$$\varepsilon_2 = ln\frac{d_2}{d_0} \quad (2)$$

### 2.4 Training

In order to train the ANN model, the data were collected from published literature and the experiment for DC01. The database comprises major and minor strain values for material thickness, yield stress, tensile strength, strength coefficient, strain hardening exponent, uniform elongation versus uniaxial strain, plane strain and biaxial strain values. In some articles, these values are given in table [30–32], but in others, they are given graphically [33–35] (stress–strain, FLC, etc.). In those studies, the graphics in the article were transferred to data collection software and the desired data were obtained this way. In this study, the data collected from the literature is given in Table 3 with respective references.

An FLC consists of two regions: negative ($\varepsilon_2^u$) and positive ($\varepsilon_2^b$) minor strain. In the ANN model, material thickness ($t$), yield stress ($YS$), ultimate tensile strength ($UTS$), strength coefficient ($K$), strain hardening exponent ($n$), and uniform elongation were used as input data. In the data collected from the literature, major strain ($\varepsilon_1^u, \varepsilon_1^b$) values were collected for different positive and negative minor strain ($\varepsilon_2^u, \varepsilon_2^b$) values for each material. These values and the slope of the curve in the positive and negative minor strain regions were calculated according to Eqs. 3 and 4. With this arrangement, $\beta^-, \beta^+$ and $FLC_0$ values are used as outputs from the ANN model.

$$\beta^- = tan^{-1}\left(\frac{\varepsilon_1^u - FLC_0}{|\varepsilon_2^u|}\right) \quad (3)$$

$$\beta^- = tan^{-1}\left(\frac{\varepsilon_1^u - FLC_0}{|\varepsilon_2^u|}\right) \quad (4)$$

Table 3. Training data from different literature works

| No | Mat. | YS | UTS | $\varepsilon$ | K | n | t | $\varepsilon_2^u/\varepsilon_1^u$ | FLC0 | $\varepsilon_2^b/\varepsilon_1^b$ | Ref. |
|---|---|---|---|---|---|---|---|---|---|---|---|
| 1 | DC01 | 204.3 | 335.9 | 24.1 | 576.3 | 0.212 | 0.6 | -0.220/0.440 | 0.281 | 0.280/0.354 | Exp. |
| 2 | Q&P 1180 | 1000.0 | 1200.0 | 14.8 | 1300 | 0.042 | 1.25 | -0.060/0.142 | 0.102 | 0.170/0.185 | [36] |
| 3 | DX54D | 167.0 | 309.0 | 22.5 | 375.2 | 0.230 | 0.75 | -0.302/0.671 | 0.351 | 0.394/0.439 | [37] |
| 4 | DP800 | 465.0 | 786.0 | 15.0 | 989.9 | 0.160 | 1.00 | -0.070/0.291 | 0.169 | 0.189/0.202 | [37] |
| 5 | DX54D +Z | 163.0 | 297.0 | 22.1 | 323.6 | 0.220 | 0.815 | -0.301/0.606 | 0.308 | 0.411/0.454 | [38] |
| 6 | DP590 | 396.8 | 761.1 | 19.7 | 1018 | 0.175 | 1.50 | -0.150/0.387 | 0.293 | 0.372/0.421 | [39] |
| 7 | IN-718 | 523.0 | 1084 | 39.3 | 1960 | 0.404 | 1.25 | -0.186/0.432 | 0.345 | 0.376/0.372 | [40] |
| 8 | TRIP600 | 350.0 | 835.8 | 26.0 | 1062.9 | 0.178 | 1.00 | -0.173/0.478 | 0.270 | 0.385/0.468 | [41] |
| 9 | DP600 | 350.0 | 734.3 | 14.2 | 1030.4 | 0.173 | 1.00 | -0.191/0.445 | 0.213 | 0.280/0.361 | [41] |
| 10 | TWIP940 | 457.2 | 960.1 | 68.9 | 2300 | 0.620 | 1.47 | -0.251/0.566 | 0.380 | 0.362/0.532 | [42] |
| 11 | TRIP780 | 508.4 | 837.0 | 16.9 | 1351 | 0.169 | 1.20 | -0.177/0.484 | 0.252 | 0.324/0.449 | [43] |

| | | | | | | | | | | | |
|---|---|---|---|---|---|---|---|---|---|---|---|
| 12 | IF steel | 202.0 | 347.2 | 11.6 | 692 | 0.321 | 0.60 | -0.165/0.541 | 0.309 | 0.119/0.436 | [44] |
| 13 | IF steel | 224.0 | 344.3 | 12.8 | 706.0 | 0.350 | 1.60 | -0.160/0.674 | 0.329 | 0.156/0.530 | [44] |
| 14 | Ferritic SS | 428.0 | 561.0 | 16.9 | 870.4 | 0.184 | 1.00 | -0.224/0.389 | 0.185 | 0.296/0.477 | [30] |
| 15 | TRIP | 422.0 | 730.0 | 35.1 | 815.7 | 0.106 | 1.00 | -0.177/0.471 | 0.260 | 0.395/0.444 | [45] |
| 16 | DP | 269.0 | 496.0 | 27.2 | 583.2 | 0.124 | 1.50 | -0.145/0.428 | 0.331 | 0.404/0.476 | [45] |
| 17 | IF | 124.0 | 311.0 | 44.1 | 357.5 | 0.170 | 1.01 | -0.323/0.699 | 0.396 | 0.300/0.464 | [45] |
| 18 | IF-HS | 204.0 | 368.0 | 36.8 | 412.0 | 0.113 | 0.84 | -0.265/0.578 | 0.325 | 0.280/0.430 | [45] |
| 19 | A0 | 290.0 | 598.0 | 38.6 | 681.65 | 0.137 | 0.82 | -0.181/0.641 | 0.381 | 0.183/0.420 | [45] |
| 20 | A3 | 305.0 | 653.0 | 46.2 | 727.4 | 0.139 | 0.80 | -0.182/0.553 | 0.363 | 0.207/0.398 | [45] |
| 21 | ZStE 180 BH | 246.0 | 343.0 | 38.9 | 364.0 | 0.063 | 0.77 | -0.271/0.599 | 0.294 | 0.414/0.442 | [45] |
| 22 | DP600 | 392.2 | 748.6 | 15.2 | 1067.2 | 0.192 | 1.20 | -0.103/0.348 | 0.175 | 0.290/0.363 | [31] |
| 23 | DP800 | 450.7 | 866.7 | 12.7 | 1185.5 | 0.168 | 1.20 | -0.097/0.290 | 0.145 | 0.259/0.279 | [31] |
| 24 | QP980 | 490.8 | 1173.4 | 16.1 | 1413.6 | 0.099 | 1.00 | -0.121/0.384 | 0.224 | 0.265/0.360 | [46] |
| 25 | JAY780Y | 526.3 | 812.9 | 12.0 | 1226.4 | 0.136 | 1.00 | -0.214/0.440 | 0.134 | 0.279/0.290 | [47] |
| 26 | QP980 | 828.0 | 1015.0 | 10.9 | 1420.0 | 0.106 | 1.60 | -0.154/0.437 | 0.203 | 0.358/0.402 | [48] |
| 27 | EDD steel | 202.0 | 337.0 | 44.0 | 677.0 | 0.304 | 1.00 | -0.077/0.366 | 0.303 | 0.099/0.377 | [49] |
| 28 | DP980 | 654 | 1027 | 8.3 | 1401 | 0.09 | 1.4 | -0.09/0.224 | 0.131 | 0.282/0.364 | [50] |
| 29 | DP600 | 340 | 587 | 19.2 | 963 | 0.184 | 1.5 | -0.254/0.429 | 0.176 | 0.342/0.376 | [51] |

### 2.5 Artificial Neural Network Analysis

A general ANN model consists of input, hidden, and output layers. Input and output layers are fixed layers in which data is requested for modelling. A consistent and large quantity of data will increase the consistency of the model. The network structure of the model can be constructed in different ways according to the number of hidden layers and neurons. There may be several hidden layers or only one. Although there is yet to be a straightforward method for determining the number of hidden layers, specific rules are considered. This number is increased according to the complexity of modelling between the input and output values of the study. For example, if the problem can be divided into stages, the number of hidden layers in the network should be increased. One, two or three hidden layers will provide sufficient results.

The weights and bias values are continuously changed to obtain outputs corresponding to the inputs given to the ANN network. This process is called the training of the network. After the training of the ANN network, new inputs that have not previously been given to the network are supplied, and the outputs are tried to be obtained with an acceptable error. Although the training error is minimal, a high error between the actual results and the outputs of the ANN in response to the new inputs indicates that the network is memorising (over-fitting).

The number of neurons in the hidden layer is one of the main parameters of the ANN model. Although there is no precise method for determining the number of neurons, it should be increased as the problem becomes more complex. The number of hidden layer

neurons in the network starts at a certain number and increases until the network provides sufficient generalisation. Too many neurons will reduce the network's generalisation ability, and the network will begin to memorise. If the number of neurons is less than necessary, the ANN cannot accurately predict the output data. Therefore, the optimal number of neurons has to be found.

In this study, an algorithm was developed in the ANN to determine the appropriate number of neurons. MATLAB 2017a was used for ANN modelling. In addition to the input and output data, the maximum and minimum numbers of neurons should be defined in the algorithm. After the normalisation of input and output data, the essential functions of the ANN network structure are determined. The following types of functions are used in the created network structures.

- Network type: feed-forward and back-propagation
- Training function: TRAINLM
- Adoption learning function: LEARNGDM
- Performance function: mean square error (MSE)

In the algorithm developed, the maximum and minimum neuron numbers are entered according to the number of hidden layers selected. All the network structures that can be formed by the number of neurons in the network are trained. From the data set, 70%, 15% and 15% of the data were randomly selected for training, testing and validating, respectively, and then the network training began. Weights and bias values were randomly assigned for each network structure formed with different neuron numbers and trained for a determined number of iterations. Although the number of training iterations for the developed algorithm was 30, this number can be increased. This initial training is called the basic training of the network. Considering the MSE value from the primary network training, the optimum network structure was determined from the network structures formed between the maximum and minimum neuron numbers in the hidden layers. The network structure was created by selecting the number of neurons with the lowest MSE value among the trained networks. The algorithm gives the MSE values for all network trials and the regression (R) graphs of the optimum network structure.

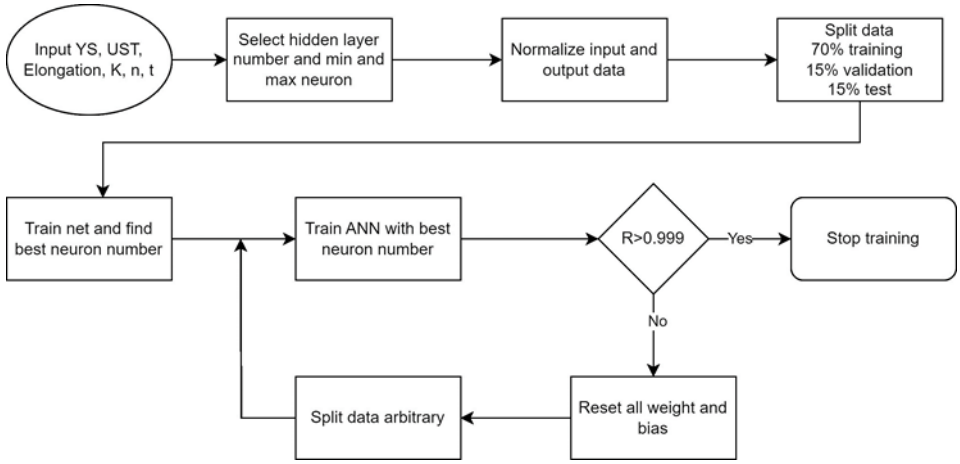


(a)

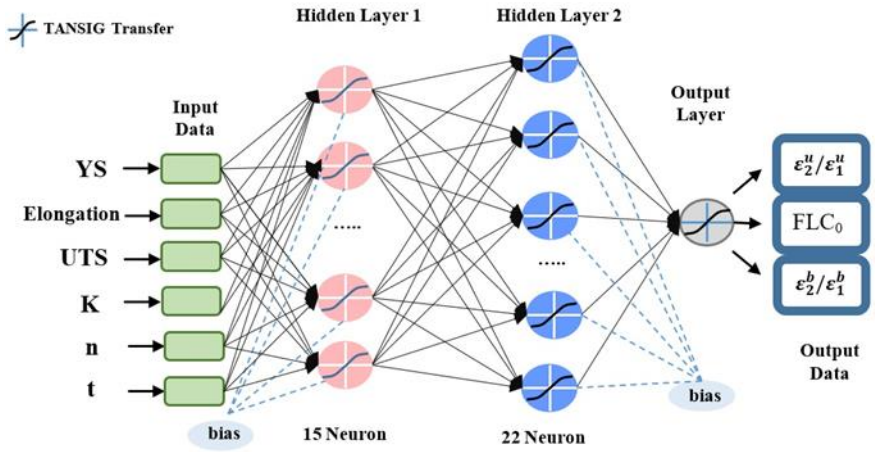


(b)

Fig 5. ANN model (a) Flow chart of the algorithm, (b) Structure of the model

The next step of the algorithm continues to train the network until it reaches the highest regression value in the specified network structure. During this training stage, the network structure is kept constant while training, testing, validation data pairs, weights and bias values are constantly changed. Thus, memorisation in the network is prevented. In the last step, the network structure with the highest regression value was recorded, and the training was terminated. The actual data and the outputs of the training results of the network are given graphically. Thus, the optimal network structure is determined by running a single algorithm for the number of layers and the neurons to be selected for each layer. The algorithm and network structure created for the ANN model is shown in Fig. 5a and 5b.

All data used in this study were normalised. The activation functions used in an ANN could give false results if mixed negative and positive numbers or huge numbers are shown in the input and output layers. Normalisation is applied to the data to prevent these errors and increase the learning speed. The definition of normalisation is the limitation of data to a specific range, such as the range [-1,0] or [0,1]. The normalisation equation is;

$$X_{new} = \frac{(X - X_{min})}{(X_{max} - X_{min})}(upperbound - lowerbound) + lowerbound \quad (5)$$

$X_{new}$, $X_{max}$ and $X_{min}$ are the restricted, maximum, and smallest values, respectively. The upper and lower bound are the upper and lower values of the range to be restricted [52]. The mean square error was used as the performance function. This function gives the average square of the difference between the network results and its outputs [53]. The MSE function is;

$$MSE = \frac{1}{N}\sum_{i=1}^{N}(y_i - z_i)^2 \quad (6)$$

Where $y_i$ is the ANN prediction, $z_i$ is the output value, and $N$ is the number of outputs.

System identification modelling was used to model the system with a MISO (multiple input, single output) model structure. Input and output parameters were arranged in the data sets and limited to [0.01–0.99] using Eq. 5. A total of 29 data pairs were used. In the

modelling process, 21 data sets were reserved for training, four for testing and four for verification. Each data sets have three outputs as $\beta^-, \beta^+$, $FLC_0$. In this study, when the model selection is made, the regression value ($R$) of the network and the comparison graphs and MSE are taken into consideration because it is necessary to check the compatibility of the model with the system by using comparison graphs to determine whether the model is successful or not. The $R$ values were calculated according to the formula in Eq. 7 [54].

$$R = \frac{n\sum x_i y_i - (\sum x_i)(\sum y_i)}{\sqrt{n\sum x_i^2 - (\sum x_i)^2}\sqrt{n\sum y_i^2 - (\sum y_i)^2}} \tag{7}$$

Here, $x_i$ is the targeted value found by experiments, and $y_i$ represents the output value of the network, in other words, the prediction. The *R-value* calculated with this formula depends on the number of specimens, the difference between the variables and the distribution of the variables. Another parameter for measuring network success is the percentage error. The formula used for percentage error is given in Eq. 8 [55]. Here, $E$ is the percentage error, $x_i$ is the targeted value found by experiments, and $y_i$ represents the output value from the network.

$$E(\%) = \frac{1}{n}\sum_i \left(\frac{|x_i - y_i|}{x_i} \cdot 100\right) \tag{8}$$

### 2.6 Sensitivity Analysis of the ANN

Artificial neural networks (ANNs) are a powerful tool used in various engineering fields, especially for solving prediction, regression and classification problems. However, ANN is generally considered a black box where it is difficult to determine the effect of each input data on any output data [56]. Sensitivity analyses are performed to determine the model outputs' critical parameters and importance levels [57]. In the sensitivity analysis results, the network output changes according to the inputs and provides information about the more sensitive parameters that need to be measured more accurately [58].

In the context of this research, understanding the influence of input parameters on the artificial neural network (ANN) model's outputs and the direction of correlations is paramount. Sensitivity analysis is a valuable tool that identifies the most influential parameters, offering several advantages. It allows for optimising predictions by emphasising precise data collection for critical parameters, ultimately enhancing the accuracy of predictions and decision-making. Additionally, sensitivity analysis streamlines experimentation efforts, conserving time and resources. Moreover, it enables potential model improvements, such as adjustments to the ANN architecture or incorporating additional data sources based on parameters showing strong correlations with the output.

Comprehending the direction of correlations between input parameters and the model's output is equally significant. Positive correlations signify that increasing an input parameter leads to an increase in the output, emphasising the need to enhance or optimise such parameters. Conversely, negative correlations indicate that increasing an input parameter decreases output, suggesting the necessity to control or minimise the parameter for better predictions. Parameters with weak or no correlation may be re-evaluated for inclusion in the model due to their limited impact on predictions.

This understanding of correlation directions facilitates the interpretation of the system's behaviour, though it's crucial to remember that correlation does not imply causation. Establishing causal relationships may require additional analyses or domain expertise. In summary, sensitivity analysis and comprehending correlation directions empower the fine-tuning of the ANN model, inform efficient data collection, and enhance the precision

and reliability of predictions, particularly in predicting forming limit curves for sheet metals.

A study on the results of comparisons of sensitivity analysis methods was made by Gevrey et al. [57]. The weight method, one of the methods examined in the study, can classify the inputs within itself and contribute to the output. This study examined the contributions of the input parameters to the FLC model created with ANN using the 'Weights' method sensitivity analysis. Garson [59] and Goh [60] proposed Weights' method. The percentages of influence of the input variable, $Q_{ik}$(%), on output value, indicating the importance of input variables, were determined by the following equation [61]:

$$Q_{ik}(\%) = \frac{\sum_{j=1}^{n}\left(\frac{|w_{ij}|}{\sum_{i=1}^{m}|w_{ij}|}|v_{jk}|\right)}{\sum_{i=1}^{m}\left(\sum_{j=1}^{n}\left(\frac{|w_{ij}|}{\sum_{i=1}^{m}|w_{ij}|}|v_{jk}|\right)\right)} \times 100 \tag{9}$$

$w_{ij}$ represents weights between the input neuron $i$ (= 1, 2, ..., $m$) and the hidden neuron $j$ (= 1, 2, ..., $n$), and $v_{jk}$ represents the weights between the hidden neuron $j$ and the output neuron $k$ (= 1, 2, ..., $l$). In this study, the input, hidden, and output neurons were 6, 15 and 3, respectively. A more detailed example of this method can be found in Ref. [57].

### 2.7 Marciniak-Kuczynski (M-K) Model

M-K model is another theoretical method to determine FLC. This model assumed that the material has an instability region which is rapidly deformed under load compared to the other areas of material (Fig. 6). The orientation of the instability region changes depending on the strain path assumed [62]. Force equilibrium for x and y direction, strain path, yield criteria and a constitutive relationship is assumed, and the strain increments in the safe and instability regions are predicted. If the strain increments of the instability region are ten times greater than the safe region, then it is assumed that the failure occurred.

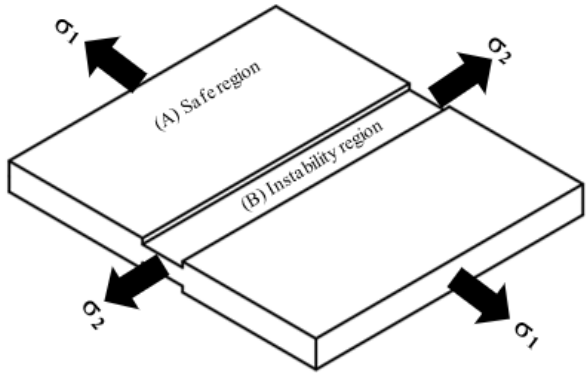


Fig. 6. Schematic sheet metal in Marciniak and Kuczynski model

FLC can be created with different strain hardening rules in the M-K model. This study used the Hollomon strain-hardening rule (Eq. 10) and von Mises yield criterion (Eq. 11) to determine FLC theoretically.

$$\sigma = K \cdot \varepsilon^{n} \tag{10}$$

$$\bar{\sigma} = \frac{1}{\sqrt{2}}\sqrt{(\sigma_1 - \sigma_2)^2 + (\sigma_2 - \sigma_3)^2 + (\sigma_3 - \sigma_1)^2} \tag{11}$$

The force equilibrium of regions A and B can be written in Eq. 12. Also, the strain increments in direction 2 are equal, as seen in Eq. 13.

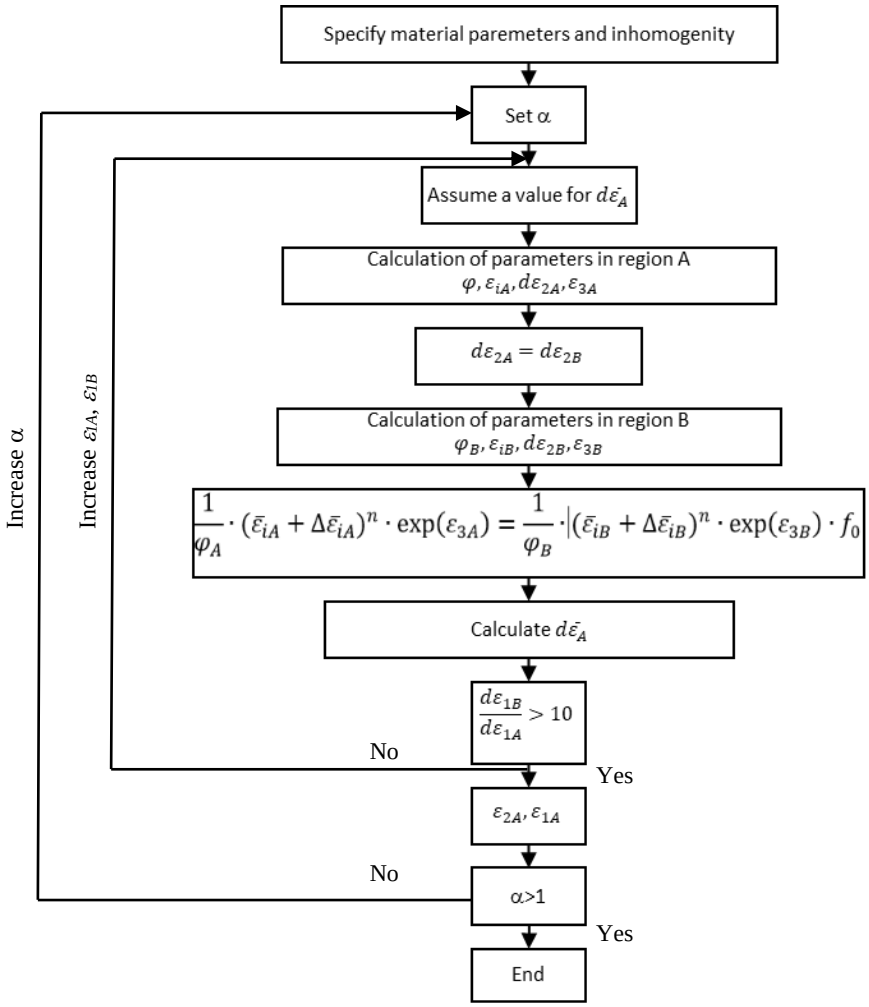


Fig. 7 Flowchart of M-K model

The force equilibrium can be written in terms of stress, strain and thickness as in Eq. 14. In this equation, $f_0$ is the inhomogeneity coefficient; in other words, the ratio of $t_B$ to $t_A$. Also, the thickness strain ($\varepsilon_3$) can be calculated from the incompressibility principle.

$$F_{1A} = F_{1B} \tag{12}$$

$$d\varepsilon_{2A} = d\varepsilon_{2B} \tag{13}$$

$$\sigma_{1A} \cdot exp(\varepsilon_{3A}) = \sigma_{1B} \cdot exp(\varepsilon_{3B}) \cdot f_0 \tag{14}$$

The ratio of effective stress to major stress is given in Eq. 15. As a result, Eq. 16 is obtained by substituting Eq. 11 and 15 in Eq. 14.

$$\varphi = \frac{\bar{\sigma}}{\sigma_1} \tag{15}$$

$$\frac{1}{\varphi_A} \cdot \bar{\varepsilon}_A^n \cdot exp(\varepsilon_{3A}) = \frac{1}{\varphi_B} \cdot \bar{\varepsilon}_B^n \cdot exp(\varepsilon_{3B}) \cdot f_0 \tag{16}$$

In Eq. 16, although the left side can be calculated simply, the right side of the equilibrium should be calculated iteratively. The Newton-Raphson method was used to determine strain increment. At the beginning of the calculation, a constant stress ratio should be defined for the safe region. By the way, Eq. 16 is arranged iteratively to obtain Eq. 17. A flowchart of the algorithm to calculate FLC is given in Fig. 7.

$$\frac{1}{\varphi_A}\cdot(\bar{\varepsilon}_{iA}+\Delta\bar{\varepsilon}_{iA})^n\cdot exp(\varepsilon_{3A})=\frac{1}{\varphi_B}\cdot(\bar{\varepsilon}_{iB}+\Delta\bar{\varepsilon}_{iB})^n\cdot exp(\varepsilon_{3B})\cdot f_0 \tag{17}$$

### 2.8 The Swift-Hill Model

It has been proven that a good simulation of the forming limit strains can be given based on the Swift diffuse instability theory and the Hill localised instability theory [45,63]. In Swift-Hill theory, the FLC's left and right sides are calculated separately based on $\alpha$. The stress-strain relationship of sheets is expressed with Hollomon's equation. For the left side of the FLC, $\varepsilon_2 < 0$, major and minor strain is given in Eq. 18 and Eq. 19 [45]. The strain hardening exponent, $n$ and anisotropy coefficient, $r$, are constant material properties in these equations.

$$\varepsilon_1=\frac{1+(1-\alpha)\cdot r}{1+\alpha}\cdot n \tag{18}$$

$$\varepsilon_2=\frac{\alpha-(1-\alpha)\cdot r}{1+\alpha}\cdot n \tag{19}$$

For the right side of FLC, $\varepsilon_2 > 0$, major and minor strains are calculated with Eq. 20 and 21.

$$\varepsilon_1=\frac{[1+(1-\alpha)\cdot r]\cdot\left[1-\frac{2\cdot r}{1+r}\cdot\alpha+\alpha^2\right]}{(1+\alpha)\cdot(1+r)\left[1-\frac{1+4\cdot r+2\cdot r^2}{(1+r)^2}\cdot\alpha+\alpha^2\right]}\cdot n \tag{20}$$

$$\varepsilon_2=\frac{[(1+r)\cdot\alpha-r]\cdot\left[1-\frac{2\cdot r}{1+r}\cdot\alpha+\alpha^2\right]}{(1+\alpha)\cdot(1+r)\left[1-\frac{1+4\cdot r+2\cdot r^2}{(1+r)^2}\cdot\alpha+\alpha^2\right]}\cdot n \tag{21}$$

### 2.9 The NADDRG Model

The North American Deep Drawing Research Group (NADDRG) suggests an empirical equation for predicting the FLC. The proposed formula enabled FLC to be quickly determined in press shops without complex experiments or theories such as M-K. According to this model, the FLC comprises two lines through the point $\varepsilon_0$ in the plane-strain state. The slopes of the lines on the left and right sides of FLC are about 45° and 20° [63]. The thickness of the sheet should be thinner than the 3.175 mm. The equation for calculating the forming limit strain $\varepsilon_0$ in terms of engineering strain is given in Eq. 22.

$$\varepsilon_0=\frac{(23.3+14.13\cdot t_0)\cdot n}{0.21} \tag{22}$$

## 3. Results and Discussion

### 3.1 Experimental FLD of steel sheet

Major and minor strain measurements were taken from the fractured specimens. Measures taken from damaged ellipses are shown with a red dot in the graph and measurements taken from the undamaged ellipse closest to the damaged ellipse are shown

in green, as seen in Fig. 8. The left and right parts of the FLC were created separately. The lines are fitted to the left and right dots. The curve formed by connecting these two lines at the intersection points was accepted as the FLC. When the graph is examined, the $FLC_0$ value for DC01 was 0.294. Due to different friction conditions during the experiment, the FLC can shift to the right or the left. DC01 sheet reached 0.4 for uniaxial strain and 0.35 for biaxial strain.

The FLCs of sheet metals may differ according to the metal type. In particular, the right side of the curve may exhibit a polynomial behaviour depending on the material type. For example, in the study of Wang et al. [64], the left side of the curve consists of a straight line, while the right side is polynomial. Another study by Mu et al. [65] similarly showed that the FLC exhibits a transition from necking to fracture in the biaxial stress region, so the curve in this region will be polynomial. The FLCs are valid for one particular material alloy, temper and gauge combination [12]. However, material properties vary from batch to batch due to production processes. Therefore, a single FLC cannot accurately describe the forming limit. Janssens et al. [66] have proposed a more general concept, the Forming Limit Band (FLB), as a region covering the entire dispersion of the Forming Limit Curves. This and similar studies show that forming limit diagrams for sheet metals with linear lines may not always give accurate results.

On the other hand, it has also been accepted as two straight lines to simplify the FLC and enable its practical use [67,68]. In addition, FLCs obtained by the NDDRG empirical method consist of two lines on the left and right. This study assumes that the FLC consists of two lines to model the FLC with artificial neural networks. In this way, the FLC can be easily expressed by a point $FLC_0$ and the slope of the two lines to the left and right of this point.

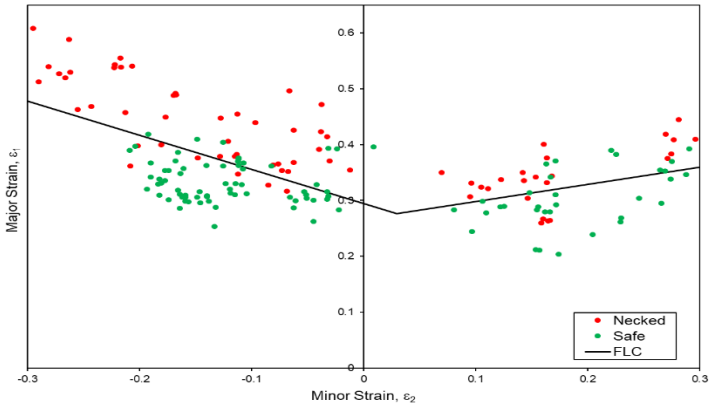


Fig. 8. Forming limit diagram of DC01

### 3.2 Artificial Neural Network Modelling Results

Experimental studies in the literature for determining FLCs, critical in metal forming processes, were modelled with an ANN. The modelling results were compared with experimentally obtained FLC values. The FLCs were determined by performing out-of-plane tests with the two steel sheets selected for the study. These FLCs were then compared with the ANN results.

This ANN study, 29 data pairs were used, considering only steel materials. In the modelling process, six parameters were determined in the input layer, and three parameters were determined in the output layer (Fig. 5b). A minimum of 15 and a maximum of 25 neurons were selected in the model structure. A total of 121 combinations of neurons were tested

in the network. The optimum number of neurons was determined by considering the MSE values of the obtained network structures. In Fig. 9, MSE values obtained from the modelling results of the network structures created with all neuron combinations after basic network training are shown. The number of neurons in the network with the lowest MSE value was determined as 15-22, and this is marked with a red dot in Fig. 9. The *R*-value obtained from the primary network training of the created network with the optimum neuron numbers is given in Fig. 10. The regression value, of approximately 0.98603, is at an acceptable level.

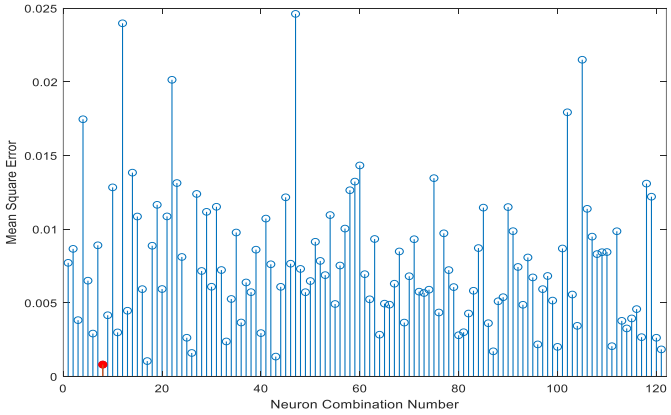


Fig. 9. MSE values of all combinations of neurons used in ANN layers

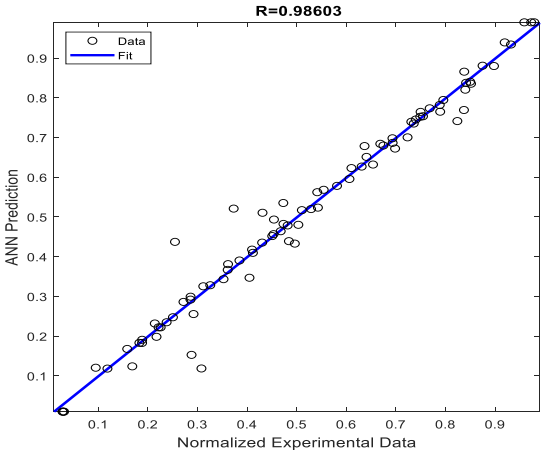


Fig. 10. The R-value after basic network training in the network structure created with the optimum number of neurons

The network structure was formed by determining the hidden layer and neuron numbers for ANN modelling. The next step of the algorithm is to re-train the network structure with optimal neuron numbers after basic network training to increase the generalisation of the network. After retraining the optimum network, the final *R* values were determined as 0.99998 for training, 0.99994 for validation and 0.99976 for testing, as shown in Fig. 11. The overall *R-value* of the network was calculated as 0.99995.

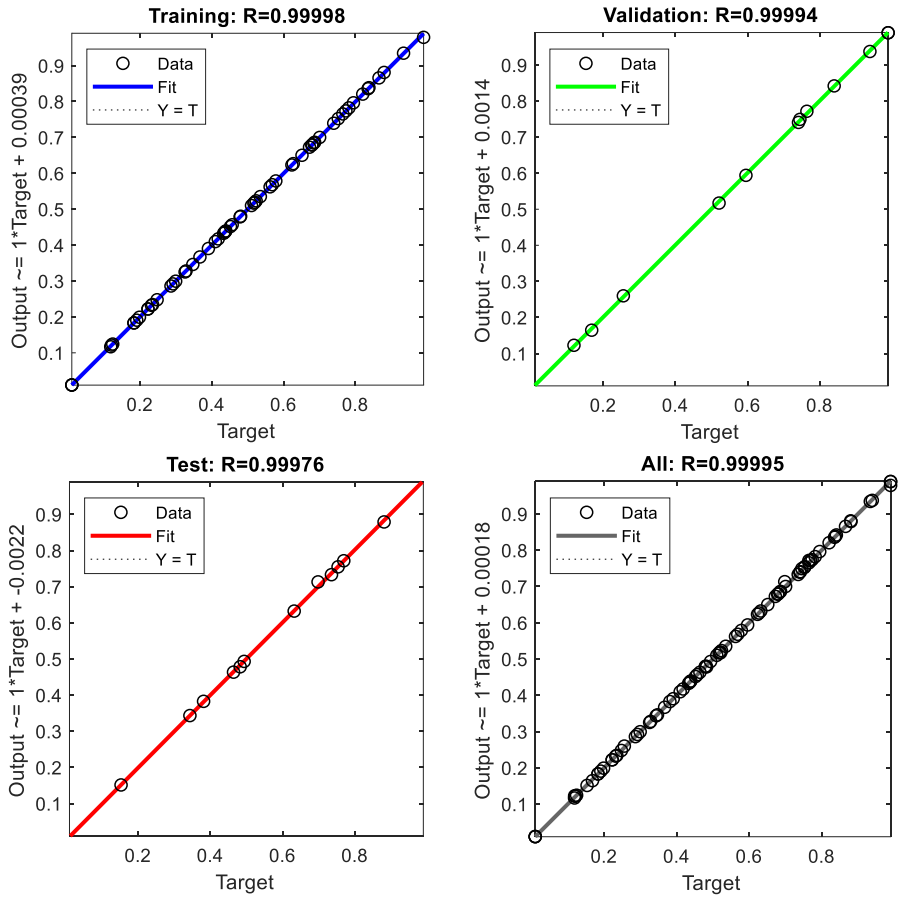


Fig. 11. The *R* values of the algorithm in the final ANN modelling

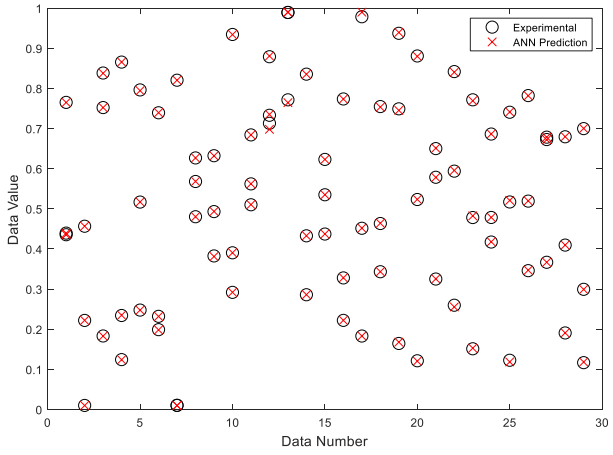


Fig. 12. Comparison of experimental results obtained from literature with ANN modelling outputs

The proximity of the *R* values to 1 indicates the success of the network structure for the modelled system. Similarly, the proximity of the *R* values of randomly selected test and

verification data to 1 reveals the consistency of the network.One of the most critical problems in ANN modelling is misleading results from the network due to memorisation. To overcome this problem, the experimentally obtained output data should be compared with the predicted output values resulting from modelling. Fig. 12 shows a graph comparing the output data with the predicted output data. The input data number (tag) given to the ANN is shown on the horizontal axis, and the input data value is shown on the vertical axis. The outputs and ANN predictions are highly consistent.

### 3.3 Contributions of input to the ANN predict

In the study, most of the selected parameters can be determined by tensile testing. Sheet thickness can be easily measured with a calliper. It is possible to get more consistent results as the number of inputs in artificial neural networks increases [69]. For this reason, six different material properties that can introduce the material were selected as input. In this section, the Weights Method determined the effect of the selected inputs on the outputs. The effects of the input parameters on the output are given in Figure 13. Accordingly, the most effective parameters on the output are *UTS* and *n* parameters, respectively. An inverse correlation between *UTS* and $FLC_0$ was reported by Belck et al. [45]. A linear correlation between $FLC_0$ and *n* is reported by Keeler and Brazier [70]. The formability also improves with increasing *n* [12,71,72]. On the other hand, the strength coefficient has the most negligible effect on the outputs, with 11.16%.

Paul grouped the material properties and estimated the FLC by choosing at least one element from each group [19]. Similar to this study, the inputs can be divided into three categories. These categories can be called experimental properties (*YS*, *UTS* and elongation), theoretical model coefficients (*K* and *n*), and sheet thickness (*t*). When evaluated as a group, the experimental properties are affected by 53.11%, the theoretical model coefficients by 31.61%, and the sheet thickness by 15.28%, respectively. Here, further studies can be made on whether the network's success can be increased by removing weak parameters such as *K*. In addition, by using different methods, it can be revealed how the inputs affect the outputs.

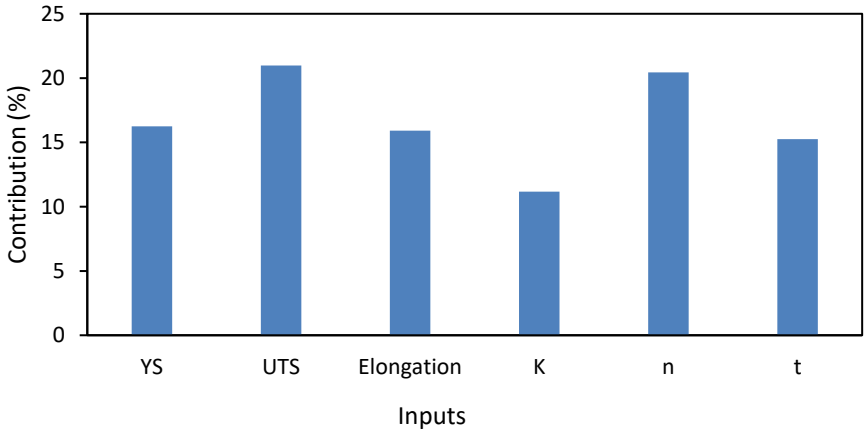


Fig. 13. The contributions of input on the ANN output

### 3.4 Comparison of experimental FLC with ANN predict

In this study, the network created was trained with the given data and success was achieved with $R = 0.99995$. The network was asked to predict the FLC from the mechanical properties of the steel sheet. The results of the trained network for DC01 are shown in Fig.

14 compared with experimental FLC. The network predicts only the $FLC_0$ point of the FLC and the slopes of the right and left sides connected to this point. The error between the experimental and predicted FLC had been calculated using Eq. 23.

$$error = \frac{\varepsilon_{1,\ theoretical} - \varepsilon_{1,exp.}}{\varepsilon_{1,exp.}} x100\% \tag{23}$$

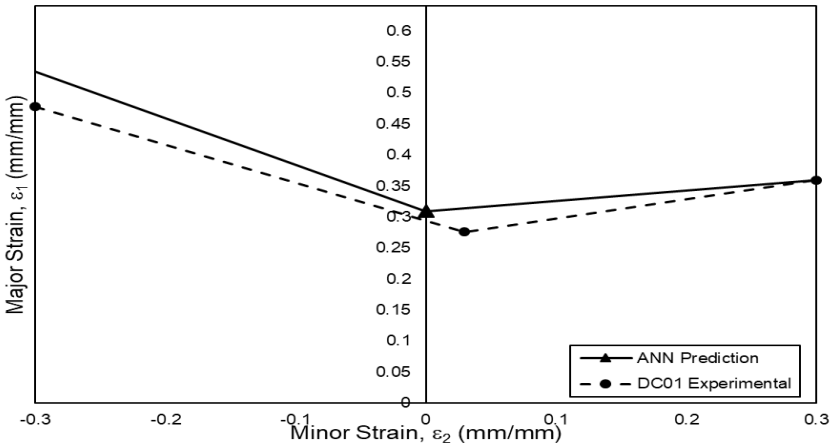


Fig. 14. Comparison of experimental FLC and ANN predictions for DC01

According to this equation, the difference in the $FLC_0$ point between ANN and the experimental result is 3.4% for DC01. In Fig. 14, the predicted and experimental results differ by only 8.5% for the left side and 4.0% for the right side on average over the whole strain region. The FLC does not give an accurate result when expressed by a single curve because, after the experiments, variables such as the region where the deformation is measured (fractured, necking or near to the necking), the marker size, and the resolution of the measurement system can change the sensitivity of the FLC. In addition, the diameter and geometry of the punch used in the test and the friction during the test may cause the FLC to shift slightly up or down. Considering all of these factors, accepting the FLC as a band gives more accurate results in terms of application. Therefore, although there are some differences in the predictions made with the ANN, these differences remain acceptable.

### 3.5 Comparison Between the Experimental, Empirical and Theoretical FLCs

This section gives theoretical, empirical, and experimental FLC for the DC01 sheet (Fig. 15). When the graphs are examined, it is seen that the results obtained with the M-K and Swift-Hill theoretical models are far from the experimental results. Although the curves obtained by NADDRG and ANN methods were slightly above the experimental curve, they were closer than the theoretical models. M-K and Swift-Hill theoretical models were below and further from the experimental curve. According to Eq. 23, when the average error between the theoretical and empirical curves is calculated along with all the minor strain values, it is seen that the ANN model gives the closest result with an average error of 10.28%. On the other hand, it is seen that the curve created with NADDRG makes a close estimation for the DC01 sheet with an average error of 15.63%.

Closer results can be obtained using different strain-hardening models and assumptions within the theoretical model. The sheets are assumed to be isotropic in the theoretical models used in this study. In addition, it is assumed that the groove, accepted on the sheet in the M-K criterion, is always perpendicular to the major stress. However, considering the

theoretical and empirical models, the results obtained with the ANN are compatible with the experimental results.

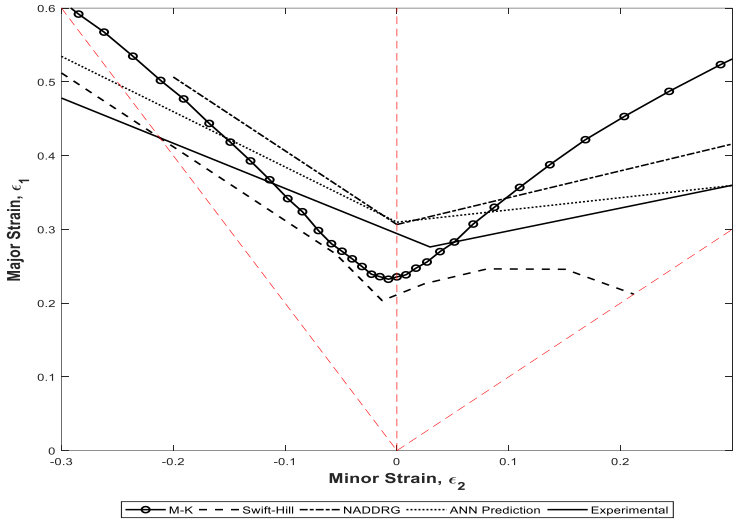


Fig. 15. The theoretical, empirical and experimental FLC of DC01

The significant difference between the theoretical models is due to the strain-hardening models and yield criteria selected for the material. Theoretical FLC is significantly influenced by strain-hardening models and yield criteria [73]. A model that gives accurate results for one material may produce inconsistent results for a different material. On the other hand, although the flow rule can very well represent the stress-strain relationships in uniaxial tensile materials, the theoretical predictions show significant deviations from the experimental FLD. A suitable calculation method depends on understanding materials' flow behaviour, assumptions for instability criteria, and perhaps other material properties and experimental factors [63].

### 3.6 Comparison between the theoretical, empirical and experimental $FLC_0$ values

A comparative bar graph of theoretical, empirical and experimental $FLC_0$ values is given in Fig. 16. The $FLC_0$ is the value that expresses the formability of the sheet in the case of plane strain and shows the lowest point of the FLC. The $FLC_0$ value is vital since crack formation and damage to the material in cold-forming processes usually occur under a plane strain state. When Fig. 16 is examined, it is seen that ANN and the NADDRG estimate the $FLC_0$ value for DC01 steel with an error of 3.4% and 2.3%, respectively. It is known that the NADDRG empirical relation gives accurate results for sheets in the deep drawing group. Other close estimates belong to the M-K and Swift-Hill theoretical models, with 21.3% and 29.2% errors, respectively. When evaluated in general, it is seen that the estimation made with ANN gives correct results like NADDRG. Compared to other methods, FLC estimation with ANN is simple and fast to be used practically in press shops if the database is expanded.

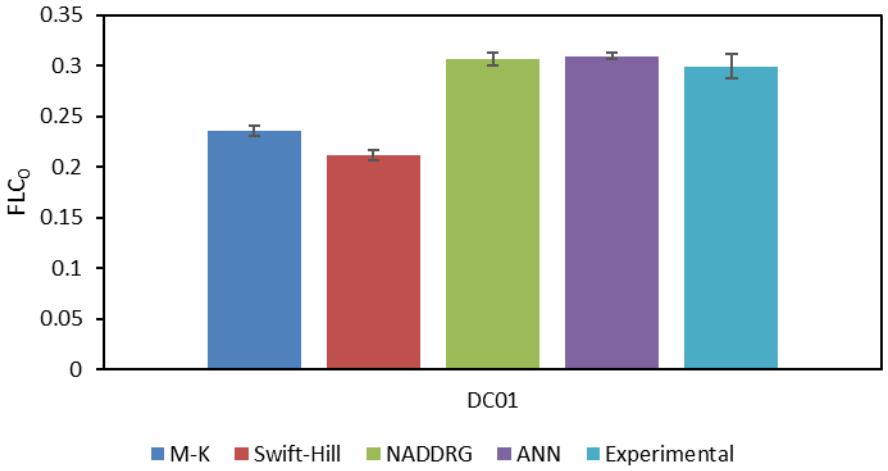


Fig. 16. Comparison between the theoretical, empirical and experimental $FLC_0$ values for DC01

## 4. Conclusions

This study demonstrated the effectiveness of an artificial neural network (ANN) model in predicting forming limit diagrams (FLDs) for sheet metals, particularly in the automotive industry. Material properties essential for this study, including sheet thickness, yield strength, ultimate tensile strength, uniform elongation, hardening exponent, and strength coefficient, were gathered and employed as inputs for the ANN model.

The key findings of this study encompass the following aspects:

- An exact ANN model with a 6-15-22-3 structure was successfully developed, yielding an R-value of 0.99995. This level of predictive accuracy holds significant implications, particularly within the automotive manufacturing domain.
- This research holds substantial practical implications, particularly for the automotive industry, which relies on accurate FLDs to ensure the quality and manufacturability of sheet metal components. With its rapid and reliable FLD predictions, the ANN model has the potential to optimise manufacturing processes, reduce material wastage, and enhance product quality.
- The accuracy of FLD predictions directly impacts manufacturing efficiency. Minor deviations in FLDs can result in significant defects or inefficiencies during production. Notably, the ANN model's capability to predict FLDs with a mere 3.4% difference from the FLD0 value highlights its potential to enhance manufacturing efficiency within the automotive sector. The difference between ANN predictions and experimental results may be acceptable for some non-critical automotive components but may fall short of industry requirements for safety-critical parts. It underscores the importance of ongoing research and development to improve predictive models to ensure the safety and reliability of automotive products.
- This study paves the way for future research and applications. While the current focus is on steel materials, the ANN model's applicability can be extended to various materials, widening its utility in the manufacturing sector. Subsequent research endeavours can explore the model's performance with different materials and further refine its capabilities.

- In summary, this research introduces a robust and efficient method for predicting FLDs, promising to revolutionise the automotive industry's quality control and manufacturing processes. The ANN model's exceptional accuracy in estimating FLDs opens avenues to enhance manufacturing efficiency and ensure product quality. As the model continues evolving and broadening its applicability to diverse materials, it will be pivotal in advancing automotive manufacturing processes. Beyond the automotive industry, the implications of this research extend to various sectors where sheet metal forming is a critical manufacturing process, heralding a new era of accuracy and efficiency in sheet metal forming and quality control. In future works, to improve the model accuracy, the input size can be widened, and ANN can estimate the polynomial curve of the FLD.

## References

[1] Ozturk F, Lee D. Experimental and numerical analysis of out-of-plane formability test. Journal of Materials Processing Technology 2005; 170: 247-53. https://doi.org/10.1016/j.jmatprotec.2005.05.010
[2] Keeler SP. Plastic instability and fracture in sheets stretched over rigid punches. 1961.
[3] Goodwin GM. Application of strain analysis to sheet metal forming problems in the press shop. SAE Transactions 1968: 380-7. https://doi.org/10.4271/680093
[4] Emmens WC. Formability; A Review of Parameters and Processes That Control, Limit or Enhance the Formability of Sheet Metal. Springer Berlin Heidelberg, 2011. https://doi.org/10.1007/978-3-642-21904-7
[5] Chang K-H. Sheet Metal Product Manufacturing and Cost Estimating Using Cad/Cae Simulation. Elsevier Inc., 2013. https://doi.org/10.1016/B978-0-12-401745-0.00006-X
[6] Brozzo P, Deluca B, Rendina R. A new method for the prediction of formability limits in metal sheets. Proc. 7th Biennal Conf. IDDR. 1972.
[7] Olsen TY. Machines for ductility testing. Proc. Am. Soc. Mater 1920; 20: 398-403.
[8] Hecker SS. A simple forming-limit curve technique and results on aluminum alloys. Int. Deep Drawing Res. Group, 7 Th Biennial Congress. Amsterdam, 1972.
[9] Marciniak Z. Stability of plastic shells under tension with kinematic boundary conditions(Stability of plastic shell under tension). Archiwum Mechaniki Stosowanej 1965; 17: 577-92.
[10] Nakazima K, Kikuma T. Forming limits under biaxial stretching of sheet metals. Testu-to Hagane 1967; 53: 455-8. https://doi.org/10.2355/tetsutohagane1955.53.10_S455
[11] Hasek V. On the strain and stress states in drawing of large un-regular sheet metal components. Berichte aus dem Institut für Umformtechnik, Universität Stuttgart, Essen, Germany, Report1973.
[12] Banabic D. Sheet Metal Forming Processes: Constitutive Modelling and Numerical Simulation. Springer Berlin Heidelberg, 2010. https://doi.org/10.1007/978-3-540-88113-1
[13] Marciniak Z, Kuczyński K. Limit strains in the processes of stretch-forming sheet metal. International Journal of Mechanical Sciences 1967; 9: 609IN1613-612IN2620. https://doi.org/10.1016/0020-7403(67)90066-5
[14] Swift H. Plastic instability under plane stress. Journal of the Mechanics and Physics of Solids 1952; 1: 1-18. https://doi.org/10.1016/0022-5096(52)90002-1
[15] Hill RT. On discontinuous plastic states, with special reference to localized necking in thin sheets. Journal of the Mechanics and Physics of Solids 1952; 1: 19-30. https://doi.org/10.1016/0022-5096(52)90003-3
[16] Gurson AL. Continuum theory of ductile rupture by void nucleation and growth: Part I-Yield criteria and flow rules for porous ductile media. Journal of engineering materials and technology 1977; 99: 2-15. https://doi.org/10.1115/1.3443401

[17] Zhang R, Shao Z, Lin J. A review on modelling techniques for formability prediction of sheet metal forming. International Journal of Lightweight Materials and Manufacture2018 Jun; doi 10.1016/j.ijlmm.2018.06.003. https://doi.org/10.1016/j.ijlmm.2018.06.003
[18] Subramani K, Alagarsamy SK, Chinnaiyan P, Chinnaiyan SN. Studies on testing and modelling of formability in aluminium alloy sheet forming. 2018; 2. https://doi.org/10.21278/TOF.42206
[19] Paul SK. Prediction of complete forming limit diagram from tensile properties of various steel sheets by a nonlinear regression based approach. Journal of Manufacturing Processes 2016; 23: 192-200. https://doi.org/10.1016/j.jmapro.2016.06.005
[20] Levy BS, Van Tyne CJ. An approach to predicting the forming limit stress components from mechanical properties. Journal of Materials Processing Technology 2016; 229: 758-68. https://doi.org/10.1016/j.jmatprotec.2015.10.027
[21] Paul SK. Controlling factors of forming limit curve: A review. Advances in Industrial and Manufacturing Engineering 2021; 2: 100033. https://doi.org/10.1016/j.aime.2021.100033
[22] Kotkunde N, Deole AD, Gupta AK. Prediction of Forming Limit Diagram for Ti-6Al-4V Alloy Using Artificial Neural Network. Procedia Materials Science 2014; 6: 341-6. https://doi.org/10.1016/j.mspro.2014.07.043
[23] Elangovan K, Sathiya Narayanan C, Narayanasamy R. Modelling of forming limit diagram of perforated commercial pure aluminium sheets using artificial neural network. Computational Materials Science 2010; 47: 1072-8. https://doi.org/10.1016/j.commatsci.2009.12.016
[24] Derogar A, Djavanroodi F. Artificial neural network modeling of forming limit diagram. Materials and Manufacturing Processes 2011; 26: 1415-22. https://doi.org/10.1080/10426914.2010.544818
[25] Forcellese A, Gabrielli F, Simoncini M. Prediction of flow curves and forming limit curves of Mg alloy thin sheets using ANN-based models. Computational Materials Science 2011; 50: 3184-97. https://doi.org/10.1016/j.commatsci.2011.05.048
[26] Dehghani K, Shafiei M A, Naeimi H. Effect of thermomechanical processing on forming limit diagrams predicted by neural networks. Materials and Manufacturing Processes 2008; 23: 829-33. https://doi.org/10.1080/10426910802384714
[27] Farahnak P, Urbánek M, Konopík P, Džugan J. Influence of thickness reduction on forming limits of mild steel DC01. International Journal of Material Forming 2020; 13: 371-81. https://doi.org/10.1007/s12289-019-01513-3
[28] ASTM E8. ASTM E8/E8M standard test methods for tension testing of metallic materials 1. Annual Book of ASTM Standards 4 2010: 1-27.
[29] ASTM E2218-02(08). Standard Test Method for Determining Forming Limit Curves. ASTM Book of Standards 2002; 02: 1-15.
[30] Bong HJ, Barlat F, Lee M-G, Ahn DC. The forming limit diagram of ferritic stainless steel sheets: Experiments and modeling. International Journal of Mechanical Sciences 2012; 64: 1-10. https://doi.org/10.1016/j.ijmecsci.2012.08.009
[31] Cardoso MC, Moreira LP. Forming Limit Analysis of DP600-800 Steels. International Journal of Chemical, Molecular, Nuclear, Materials and Metallurgical Engieering 2015; 9: 1062-9.
[32] Paul SK. Theoretical analysis of strain- and stress-based forming limit diagrams. The Journal of Strain Analysis for Engineering Design 2013; 48: 177-88. https://doi.org/10.1177/0309324712468524
[33] Zhang C, Leotoing L, Guines D, Ragneau E. Theoretical and numerical study of strain rate influence on AA5083 formability. Journal of Materials Processing Technology 2009; 209: 3849-58. https://doi.org/10.1016/j.jmatprotec.2008.09.003

[34] Jie M, Cheng CH, Chan LC, Chow CL. Forming limit diagrams of strain-rate-dependent sheet metals. International Journal of Mechanical Sciences 2009; 51: 269-75. https://doi.org/10.1016/j.ijmecsci.2009.01.007
[35] Abedrabbo N, Pourboghrat F, Carsley J. Forming of aluminum alloys at elevated temperatures - Part 2: Numerical modeling and experimental verification. International Journal of Plasticity 2006; 22: 342-73. https://doi.org/10.1016/j.ijplas.2005.03.006
[36] Cramer J, Adams D, Miles M et al. Effect of Strain Path on Forming Limits and Retained Austenite Transformation in Q&P 1180 Steel. Materials Science and Engineering: A2018 Jul 19. https://doi.org/10.1016/j.msea.2018.07.062
[37] Affronti E, Merklein M. Analysis of the bending effects and the biaxial pre-straining in sheet metal stretch forming processes for the determination of the forming limits. International Journal of Mechanical Sciences 2018; 138-139: 295-309. https://doi.org/10.1016/j.ijmecsci.2018.02.024
[38] Sklad MP, Atzema EH, Schouten FJ, de Bruine M, Emrich A. Experimental Study of forming limits in multistage deformation processes. Proceedings of IDDRG 2008, International Conference. 2008: 1-12.
[39] Ma B, Liu ZG, Jiang Z, Wu X, Diao K, Wan M. Prediction of forming limit in DP590 steel sheet forming: An extended fracture criterion. Materials & Design 2016; 96: 401-8. https://doi.org/10.1016/j.matdes.2016.02.034
[40] Prasad KS, Kamal T, Panda SK, Kar S, Murty SVSN, Sharma SC. Finite Element Validation of Forming Limit Diagram of IN-718 Sheet Metal. Materials Today: Proceedings 2015; 2: 2037-45. https://doi.org/10.1016/j.matpr.2015.07.174
[41] Uthaisangsuk V, Prahl U, Bleck W. Characterisation of formability behaviour of multiphase steels by micromechanical modelling. International Journal of Fracture 2009; 157: 55-69. https://doi.org/10.1007/s10704-009-9329-4
[42] Chung K, Ahn K, Yoo D-H, Chung K-H, Seo M-H, Park S-H. Formability of TWIP (twinning induced plasticity) automotive sheets. International Journal of Plasticity 2011; 27: 52-81. https://doi.org/10.1016/j.ijplas.2010.03.006
[43] Panich S, Barlat F, Uthaisangsuk V, Suranuntchai S, Jirathearanat S. Experimental and theoretical formability analysis using strain and stress based forming limit diagram for advanced high strength steels. Materials & Design 2013; 51: 756-66. https://doi.org/10.1016/j.matdes.2013.04.080
[44] Narayanasamy R, Narayanan CS. Forming limit diagram for Indian interstitial free steels. Materials & Design 2006; 27: 882-99. https://doi.org/10.1016/j.matdes.2005.03.014
[45] Bleck W, Deng Z, Papamantellos K, Gusek CO. A comparative study of the forming-limit diagram models for sheet steels. 1998; 83: 223-30. https://doi.org/10.1016/S0924-0136(98)00066-1
[46] Mohammed B, Park T, Kim H, Pourboghrat F, Esmaeilpour R. The forming limit curve for multiphase advanced high strength steels based on crystal plasticity finite element modeling. Materials Science and Engineering: A 2018; 725: 250-66. https://doi.org/10.1016/j.msea.2018.04.029
[47] Panich S, Suranuntchai S, Jirathearanat S, Uthaisangsuk V. A hybrid method for prediction of damage initiation and fracture and its application to forming limit analysis of advanced high strength steel sheet. Engineering Fracture Mechanics 2016; 166: 97-127. https://doi.org/10.1016/j.engfracmech.2016.08.025
[48] Gao X, Mın J, Zhang L, Lı Q, Lıan C, Lın J. Prediction and Experimental Validation of Forming Limit Curve of a Quenched and Partitioned Steel. Journal of Iron and Steel Research, International 2016; 23: 580-5. https://doi.org/10.1016/S1006-706X(16)30091-7

[49] Goud RR, Prasad KE, Singh SK. Formability Limit Diagrams of Extra-deep-drawing Steel at Elevated Temperatures. Procedia Materials Science 2014; 6: 123-8. https://doi.org/10.1016/j.mspro.2014.07.014
[50] Zhang L, Min J, Carsley JE, Stoughton TB, Lin J. Experimental and theoretical investigation on the role of friction in Nakazima testing. International Journal of Mechanical Sciences 2017; 133: 217-26. https://doi.org/10.1016/j.ijmecsci.2017.08.020
[51] Maris C, Hassannejadasl A, Green DE et al. Comparison of quasi-static and electrohydraulic free forming limits for DP600 and AA5182 sheets. Journal of Materials Processing Technology 2016; 235: 206-19. https://doi.org/10.1016/j.jmatprotec.2016.04.028
[52] Nasr GE, Badr EA, Joun C. Backpropagation neural networks for modeling gasoline consumption. Energy Conversion and Management2003; doi 10.1016/S0196-8904(02)00087-0. https://doi.org/10.1016/S0196-8904(02)00087-0
[53] Ahmadloo E, Azizi S. Prediction of thermal conductivity of various nanofluids using artificial neural network. International Communications in Heat and Mass Transfer 2016; 74: 69-75. https://doi.org/10.1016/j.icheatmasstransfer.2016.03.008
[54] Chapra S, Canale R, Heperkan H. Yazılım ve Programlama Uygulamalarıyla Mühendisler Için Sayısal Yöntemler. istanbul: Literatür Yayıncılık, 2003.
[55] Eğrioğlu E, Aladağ ÇH, Günay S. A new model selection strategy in artificial neural networks. Applied Mathematics and Computation 2008; 195: 591-7. https://doi.org/10.1016/j.amc.2007.05.005
[56] Cao M, Alkayem NF, Pan L, Novák D. Advanced Methods in Neural Networks-Based Sensitivity Analysis with their Applications in Civil Engineering. Artificial Neural Networks - Models and Applications2016 Oct. https://doi.org/10.5772/64026
[57] Gevrey M, Dimopoulos I, Lek S. Review and comparison of methods to study the contribution of variables in artificial neural network models. Ecological Modelling 2003; 160: 249-64. https://doi.org/10.1016/S0304-3800(02)00257-0
[58] Shojaeefard MH, Akbari M, Tahani M, Farhani F. Sensitivity analysis of the artificial neural network outputs in friction stir lap joining of aluminum to brass. Advances in Materials Science and Engineering 2013. https://doi.org/10.1155/2013/574914
[59] Garson D. Interpreting neural network connection weights. Artificial Intelligence Expert 1991; 6: 47-51.
[60] Goh ATC. Back-propagation neural networks for modeling complex systems. Artificial Intelligence in Engineering 1995; 9: 143-51. https://doi.org/10.1016/0954-1810(94)00011-S
[61] Song K, Park YS, Zheng F, Kang H. The application of Artificial Neural Network (ANN) model to the simulation of denitrification rates in mesocosm-scale wetlands. Ecological Informatics 2013; 16: 10-6. https://doi.org/10.1016/j.ecoinf.2013.04.002
[62] Kasikci T. Experimental investigation of key assumptions in analytical failure criteria for sheet metal forming. 2010.
[63] Slota J, Spišák E. Comparison of the forming-limit diagram (FLD) models for drawing quality (DQ) steel sheets. Metalurgija 2005; 44: 249-53.
[64] Wang Y, Zhang C, Yang Y et al. The integration of through-thickness normal stress and friction stress in the M-K model to improve the accuracy of predicted FLCs. International Journal of Plasticity 2019; 120: 147-63. https://doi.org/10.1016/j.ijplas.2019.04.017
[65] Mu L, Jia Z, Ma Z, Shen F, Sun Y, Zang Y. A theoretical prediction framework for the construction of a fracture forming limit curve accounting for fracture pattern transition. International Journal of Plasticity 2020; 129: 102706. https://doi.org/10.1016/j.ijplas.2020.102706
[66] Janssens K, Lambert F, Vanrostenberghe S, Vermeulen M. Statistical evaluation of the uncertainty of experimentally characterised forming limits of sheet steel. Journal of

Materials Processing Technology 2001; 112: 174-84. https://doi.org/10.1016/S0924-0136(00)00890-6
[67] Chen X, Niu C, Lian C, Lin J. The Evaluation of Formability of the 3rd Generation Advanced High Strength Steels QP980 based on Digital Image Correlation Method. Procedia Engineering 2017; 207: 556-61. https://doi.org/10.1016/j.proeng.2017.10.1020
[68] Patel G, Kakandikar G. Investigations on Effect of Thickness and Rolling Direction of Thin Metal Foil on Forming Limit Curves in Microforming Process. LTD, 2020. https://doi.org/10.1016/B978-0-12-819496-6.00007-5
[69] Abdelbary A. Prediction of Wear in Polymers and Their Composites., 2014. https://doi.org/10.1533/9781782421788.185
[70] Keeler SP, Brazier WG. Relationship between Laboratory Material Characterization and Press-Shop Formability. Microalloying 1975; 75: 517-30.
[71] Ghazanfari A, Assempour A. Calibration of forming limit diagrams using a modified Marciniak-Kuczynski model and an empirical law. Materials & Design 2012; 34: 185-91. https://doi.org/10.1016/j.matdes.2011.07.057
[72] Z. Marciniak, J.L. Duncan SJH. Mechanics of Sheet. Butterworth Heinemann, 2002.
[73] Kotkunde N, Srinivasan S, Krishna G, Gupta AK, Singh SK. Influence of material models on theoretical forming limit diagram prediction for Ti-6Al-4V alloy under warm condition. Transactions of Nonferrous Metals Society of China 2016; 26: 736-46. https://doi.org/10.1016/S1003-6326(16)64140-7